applied sciences

MDPI

Article

Methods to Reproduce In-Plane Deformability of Orthotropic Floors in the Finite Element Models of Buildings

Giada Frappa *, Igino Pitacco, Simone Baldassi and Margherita Pauletta

Polytechnic Department of Engineering and Architecture, University of Udine, 33100 Udine, Italy; igino.pitacco@uniud.it (I.P.); baldassi.simone@spes.uniud.it (S.B.); margherita.pauletta@uniud.it (M.P.)
* Correspondence: giada.frappa@uniud.it

Abstract: In the modelling of reinforced concrete (RC) buildings, the rigid diaphragm hypothesis to represent the in-plane behavior of floors was and still is very commonly adopted because of its simplicity and computational cheapness. However, since excessive floor in-plane deformability can cause a very different redistribution of lateral forces on vertical resisting elements, it may be necessary to consider floor deformability. This paper investigates the classical yet intriguing question of modeling orthotropic RC floor systems endowed with lightening elements by means of a uniform orthotropic slab in order to describe accurately the building response under seismic loads. The simplified method, commonly adopted by engineers and based on the equivalence between the transverse stiffness of the RC elements of the real floor and those of the orthotropic slab, is presented. A case study in which this simplified method is used is also provided. Then, an advanced finite element (FE)-based method to determine the elastic properties of the equivalent homogenized orthotropic slab is proposed. The novel aspect of this method is that it takes into account the interaction of shell elements with frame elements in the 3D FE model of the building. Based on the results obtained from the application of this method to a case study, a discussion on the adequacy of the simplified method is also provided.

Keywords: RC floors; orthotropic floors; lightening elements; shell element; in-plane deformability; finite element model; homogenization method

Citation: Frappa, G.; Pitacco, I.; Baldassi, S.; Pauletta, M. Methods to Reproduce In-Plane Deformability of Orthotropic Floors in the Finite Element Models of Buildings. *Appl. Sci.* **2023**, *13*, 6733. https://doi.org/10.3390/app13116733

Academic Editors: Sara Cattaneo and Manuela Alessandra Scamardo

Received: 10 May 2023
Revised: 26 May 2023
Accepted: 30 May 2023
Published: 31 May 2023

1. Introduction

The structural behavior of reinforced concrete (RC) buildings under seismic actions is influenced by floors' in-plane stiffness, which has a crucial role in the distribution of inertia forces to vertical structural elements. Such distribution of forces does not depend on the absolute floor stiffness but rather on the ratio between the floor stiffness and the lateral stiffness of vertical elements [1].

In order to guarantee that inertia forces arising in the building distribute among vertical resistant elements proportionally to their lateral stiffness, modern building codes recommend that floors subject to seismic actions are designed to behave as rigid diaphragms.

The main geometric factors influencing floor in-plane stiffness are the floor thickness and shape ratio (length/width), the building plan geometry (i.e., rectangular, U-shaped, or L-shaped), the presence of openings within the floor, and the position of shear walls in the building plan [2–5].

The main worldwide building codes [6–13] provide qualitative and quantitative criteria to evaluate the adequacy of the rigid floor hypothesis. Qualitative criteria are primarily related to the shape of the diaphragm, while quantitative criteria set bounds to the in-plane deformation of the diaphragm. For instance, the Italian code mandates checking the rigid floor assumption when the building has an elongated- or noncompact-shaped plan or when there are shear walls with high lateral stiffness [8]. It also states that diaphragms can be

considered infinitely rigid if, when their actual in-plane flexibility is modeled, the horizontal displacements nowhere exceed those resulting from the rigid diaphragm assumption by more than 10% of the corresponding absolute horizontal displacements.

In existing Italian RC buildings, the most widespread floor typologies are the one-way joist systems made by a monolithic combination of a latticework of RC beams filled with regularly spaced ribs (joists) and a top slab with permanent light-weight fillers (usually hollow bricks) between the ribs.

For this floor system, the code states that the rigid floor assumption can only be adopted if the slab thickness is not smaller than 40 mm. In existing buildings, designed only for gravity loads, this condition is not always satisfied, as it occurs in the two case-studies analyzed in [14]. Moreover, it is not unusual to deal with buildings having high length-to-width ratios [15], in-plan irregular structural patterns, and/or shear walls not uniformly distributed within the building plan [14]. For such buildings, the in-plane floor deformability could determine a larger demand of both strength and ductility to some structural elements as compared to the case of rigid floors [16–22].

In all the mentioned cases, the actual in-plane floor deformability may be not negligible. Furthermore, for buildings seismically retrofitted with external stiffening frames connected to the building structure along the perimeter, it may be necessary to take into account the effect of floor in-plane deformability to correctly evaluate the intervention effectiveness.

For the seismic analysis of buildings, 3D FE models realized with frame and shell elements are commonly used due to their practicality and computational efficiency. In these models, the complex floor systems are represented by equivalent uniform orthotropic slabs discretized by shell elements with a prevalent membrane behavior (the bending plate part of the shell is not important).

The problem of determining the characteristics of an equivalent orthotropic slab that reproduces the behavior of a ribbed plate (homogenization problem) is a rather old one. The method fundamentals were established in a 1914 paper by Huber [23] regarding the bending behavior of reinforced concrete plates with steel ribs. A detailed bibliography on ribbed and corrugated plates homogenization, updated up to about 1970, is contained in the introduction of the book by Troiski [24], in which several concrete homogenization problems are also discussed, albeit limited to the flexural case.

Since the 1960s, the development and diffusion of fiber-reinforced composite materials has promoted the definition development of homogenization techniques built on a rigorous mathematical basis. These techniques are based on the identification of a representative volume element (RVE) of the material (structure) either in statistical terms or as a periodically repeating cell. The RVE is a material (structure) portion that is considered sufficiently large with respect to inhomogeneities but small with respect to the whole body (structure) and that is able to describe the properties of any macroscopic portion of the body (see [25] for an introduction on the subject).

More recently, a very elegant numerical homogenization technique, based on the strain energy equivalence and static condensation of degrees of freedom of a solid model of the RVE, was proposed by Biancolini [26]. This technique was applied to sandwich panels of corrugated cardboards by Garbowski et al. [27]. Marek et al. [28] compared the efficacy of this technique with the classical laminated plate theory for corrugated cardboard homogenization. Staszak et al. applied the same technique to bubble deck concrete slabs [29] and filigree ceiling elements [30], determining the equivalent properties of a flat shell able to simulate both the membrane and the flexural behavior.

Although homogenization techniques have solid mathematical foundations, their application to the case of complex floor systems is anything but rigorous. For instance, in the one-way joists system mentioned above, the RVE is easily identified as the portion of floor bounded by a single square cell of the latticework of RC beams and composed of the joists, the RC slab, and lightening elements. However, even if the equivalent properties of the single cell can be estimated with arbitrary precision by means of a finite element model, it cannot be concluded that these are the equivalent properties of the entire floor.

The reason for this is simple: one of the fundamental homogenization hypotheses is not verified, as the dimension of the cell is of the same order of magnitude as the whole floor since a typical floor system is usually composed of a small number of cells that are arranged along a few (1–6) rows and bays.

Although the importance of correctly evaluating the in-plane floor stiffness is well recognized, in the literature, the studies proposing an operational method to derive the mechanical properties of equivalent slab are few. Actually, most of the research works dealing with in-plane floor deformability investigate the main factors influencing the relevance of floor deformability effects on the building structural behavior. These factors are the building plan shape, the floor length-to-width ratio, the ratio between the building height and the floor length, the number of stories, and the position of the shear walls ([1–5,16–36]).

In both the research works presented in [31,32], which propose a method to derive the properties of the equivalent shell elements, a numerical approach is adopted. In these works, the equivalent thicknesses of shell elements in their main directions [31] or the equivalent material compressive elastic moduli [32] are determined from the comparison of two FE models of the floor: the first realized with solid elements and the second with shell elements. The displacements induced by horizontal loads are used as comparison parameters. In both works, the floor in-plane bending behavior is investigated in the presence of distributed horizontal forces applied to the floor edge. To obtain the equality of the maximum displacements of the two FE models [31] or the maximum to minimum in-plane displacements ratio [32], the properties of the equivalent slab are found through an iterative method.

Neither of the proposed numerical methods takes into account how the interaction between shell-type elements and frame-type elements, used to reproduce the frame structure, occurs in the 3D FE model of the building.

In practice, the method based on the equivalence between the transverse stiffness (in two orthogonal plane directions) of the RC elements of the real floor and that of the orthotropic slab is commonly adopted by engineers. This simplified analytical-based method does not consider the in-plane shear stiffness equivalence. If the shell element thickness is set equal to that of the RC floor's slab, the in-plane shear stiffness is given by the product of its thickness and the shear elastic modulus of the concrete. This simplified approach is described in Section 2, and a particular case study in which this method is suitable to reproduce a floor's in-plane deformability is covered in Section 2.2.

Section 3 sets out the theoretical basis of a numerical method to determine the linear elastic properties of the equivalent homogenized orthotropic slab, and in Section 4, the method is applied.

The novel aspect of this method is that it takes into account the interaction of shell elements with frame elements in the 3D FE model of the building. The equivalence between the in-plane stiffness of the orthotropic slab and that of the real orthotropic floor is assessed on the basis of the solid FE model of the floor with consideration given to the deformation patterns of the floor cell consistent with those occurring in the FE model due to seismic actions.

2. Simplified Analytical-Based Method

2.1. Method

In practice, to reproduce the in-plane deformability of orthotropic floors, engineers usually take account of the orthotropy by adopting shell elements with different in-plane (membrane) stiffnesses in the main directions and by neglecting the contribution of lightening elements. Consequently, the stiffness in the joists' direction, $k_{eq,j}$, is obtained by imposing an equality between the transverse stiffness of shell elements and that of floor RC elements (i.e., the joists and the slab). In the orthogonal direction, the in-plane stiffness $k_{eq,t}$ is usually taken to be equal to that of the floor RC slab, neglecting any contribution of joists.

This procedure is basically derived from the schematization of the floor constitutive elements through single degrees of freedom (DOF) springs with elastic axial stiffness equal to that of each element. The in-plane axial stiffness of the equivalent 2D element is obtained by the sum of the elastic axial stiffness of the springs representing each floor element. With k_s, k_j, and k_{le} denoting the axial stiffness of the slab, the joists, and the lightening elements, respectively, the value of $k_{eq,j}$ is determined as

$$k_{eq,j} = k_s + k_j + k_{le}, \tag{1}$$

where the springs' stiffnesses are evaluated by the product of the Young's modulus of the material and the cross-section area of the element. With E_c and E_{le} denoting the Young's moduli of the concrete and lightening elements, respectively, and A_s, A_j, and A_{le} being the transverse area of the slab, the joists, and the lightening elements, respectively, Equation (1) becomes

$$k_{eq,j} = E_c \cdot (A_s + A_j) + E_{le} \cdot A_{le} \tag{2}$$

If the contribution of lightening elements is neglected, it becomes

$$k_{eq,j} = E_c \cdot (A_s + A_j). \tag{3}$$

Similarly, the value of $k_{eq,t}$ is determined as

$$k_{eq,t} = E_c \cdot A_s. \tag{4}$$

If the thickness of the shell elements is set equal to that of the RC floor slab, the in-plane stiffness of the shell element in the direction orthogonal to joists is simply equal to $k_{eq,t}$. However, if this were the case, the stiffness in the joist direction would also be equal to $E_c \cdot A_s$. Hence, a stiffness modifier k_{mod} is commonly used in the applications chosen so that

$$k_{mod} \cdot E_c \cdot A_s = k_{eq,j} \tag{5}$$

Since the in-plane shear stiffness equivalence is not forced, the equivalent shell element may not be suitable to reproducing the actual in-plane stiffness of floors under seismic actions. However, the simplified method can certainly be useful in those cases in which floors are subjected to constant axial stresses along the edges. This situation may occur, for instance, in inclined roof floors under static loads.

In the next subsection, the effect of floors' in-plane stiffness on the forces arising in the structural elements of a real case study with inclined floors, subject to gravitational loads, is investigated.

2.2. Case Study

2.2.1. Description

Let us consider the roof of an existing RC building used for sporting activities. The FE model of the roof made using SAP2000 [37] software is shown in Figure 1.

The roof plane is bounded by two straight parallel lines in one direction and by two circumference arcs in the transverse direction. Considering a reference system with the origin located at the center of the circumference to which, ideally, the curved edges belong to, the X axis is taken parallel to the straight sides while the Y axis is orthogonal to X. Along X and Y, the roof has dimensions of about 34×18 m^2.

The bearing structure of the roof is made by 24 trusses disposed radially with respect to the origin of the reference axes and equally spaced. The trusses are, in turn, composed of three structural elements—a top beam, an inclined bottom chord, and a vertical strut—which are connected to each other to form a triangular static scheme. The top beam has a slight 6% slope with respect to the horizontal plane.

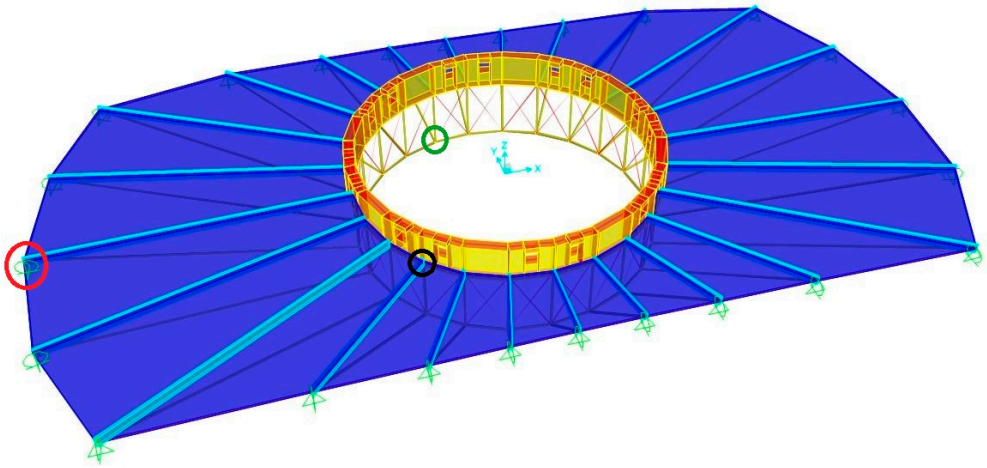

Figure 1. 3D view of the FE model of the case study's roof.

The top beam is made of a composite steel-concrete element (Figure 2), with a HEA200 profile connected on the top to a rectangular cross-section RC element of dimensions 60 × 22 cm^2. The connection is made with steel U-shaped connectors welded to the top flange of steel profiles along its whole length. The inclined bottom chords and the vertical struts are, instead, made of circular hollow steel profiles with a diameter of 9 cm and a thickness of 6.5 mm.

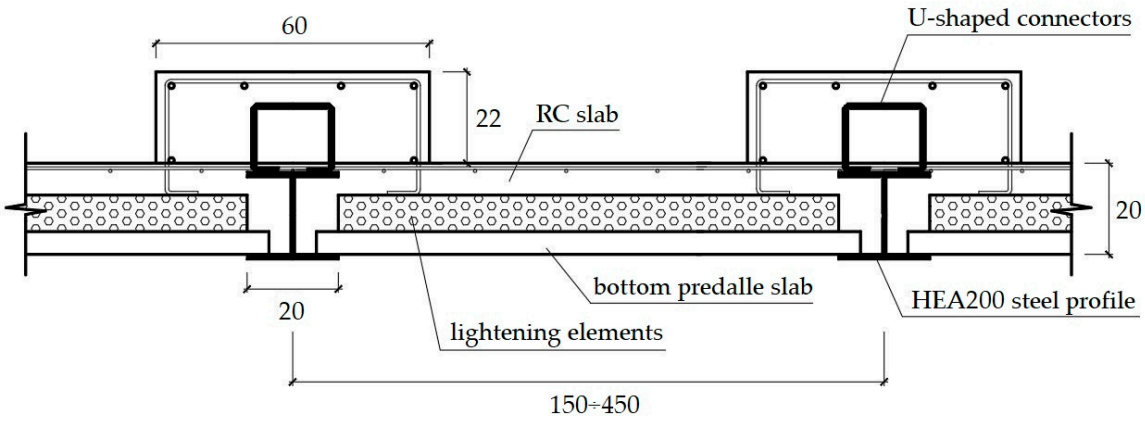

Figure 2. Connection between the floor and the top beams of the radial trusses (dimensions are in cm).

Along the perimeter of the building, the radial trusses are connected to the RC perimeter beams corresponding to the nodes between the top beam and the bottom chord (Figure 1), where one of these nodes is circled in red. In the center of the roof, the nodes between the bottom chord and the vertical strut of trusses are connected to each other with 24 steel profiles, constituting a polygonal truss lying in a horizontal plane. In Figure 1, one of these nodes is highlighted with a green circle. These profiles have the same cross-section of vertical struts and bottom chords. Conversely, the nodes between the top beam and the vertical strut, one of which is circled in black in Figure 1, are connected to each other by a circular-shaped RC beam (emergent beam in Figure 1), with rectangular cross-section dimensions of 40 × 140 cm^2. In this beam, there are 16 square holes of side 50 cm.

Moreover, the nodes between the top beams and the vertical struts are connected to the bottom nodes of the adjacent beams belonging to the polygonal truss by means of diagonal ties, composed of steel bars 20 mm in diameter, which are represented in red in Figure 3.

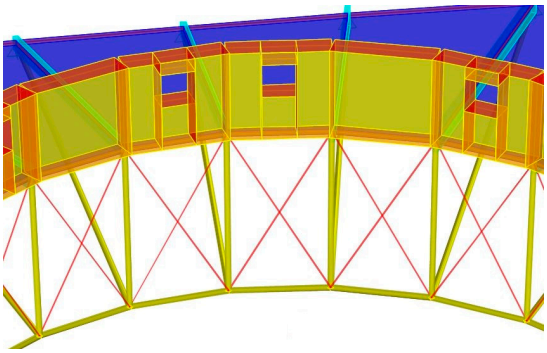

Figure 3. Diagonal ties connecting the nodes of the adjacent radial trusses.

The effect exerted by RC perimeter beams of the building on the radial trusses is modelled through restraints that prevent translations along the axial direction of the perimeter beams, assuming these beams are inextensible. These restraints also prevent the translations along the vertical direction due to the high flexural stiffness of perimeter beams toward vertical loads. Conversely, translations orthogonal to the perimeter beams axis are allowed due to the finite flexural stiffness of the perimeter beams under bending actions in the horizontal plane.

The roof is composed of 24 floor cells, each of which is bounded by the top beams of two adjacent radial trusses and by the portions of the perimeter beam and the circular-shaped RC beam between the considered radial trusses. The floors are made of pre-cast predalles type slabs with polystyrene lightening elements placed above, completed by casted-in-place RC joists with a slab on the top. Predalles slabs are 4 cm thick and 120 cm wide and are installed with their longitudinal axis orthogonal to the bisector of the angle between the longitudinal axes of the radial trusses bounding the floor cell, resting on the bottom flanges of HEA200 profiles. Their length varies according to the function of their position and is equal to the average distance between the radial trusses supporting them (Figure 2). Joists are 8 cm high and 12 cm or 24 cm wide, depending on whether they are located in the midspan of predalles slab or straddling two consecutive predalles slabs, respectively. The spacing between the joists is equal to 60 cm. From the above description, it can be gathered that the dimensions of the lightening elements in the floor cross-section are 42×8 cm^2. The top flanges of HEA200 profiles are fully embedded in the topping RC slab of the floor, and the transverse reinforcement of the slab passes over the flanges, as shown in Figure 2. Hence, the slab is continuous all over the roof surface and bounded by the perimeter beams and the circular-shaped RC beam.

Due to the presence of a space between the adjacent bottom predalles slabs (Figure 4), they are not in contact along their longitudinal edges. As a consequence, bottom predalles slabs do not contribute to the transmission of compression or tensile stresses along the direction orthogonal to their longitudinal axis. Therefore, their contribution to axial in-plane stiffness of floors along the circumferential direction is null.

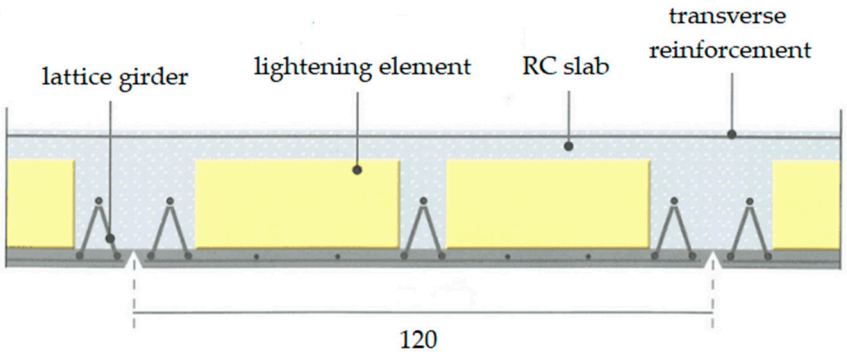

Figure 4. Space between adjacent bottom predalles slabs.

A steel-framed structure with a 16-edge pyramidal shape and cellular polycarbonate panels is anchored to the top side of the circular-shaped RC beam, serving as a covering of the central hole.

Under the gravitational loads, the circular-shaped RC beam and the radial trusses undergo downward vertical displacement. Due to the radial configuration of the roof-bearing structure and the translations of the radial trusses ending at the connection with the perimeter beams orthogonal to the perimeter beams' axes, in the horizontal plane, the points at the bottom of the circular-shaped RC beam undergo radial horizontal displacement. In particular, these displacements are outward (from the center) for the beam portions connected to the shorter radial trusses and inward for those connected to the longer radial trusses. At the same time, the ends of the radial trusses connected to the perimeter beams move outward, orthogonally to the perimeter.

Due to the kinematic behavior of the bearing structure, the floors are subject to in-plane stress states. Hence, floors, due to their in-plane stiffness, interact with the roof bearing structure, influencing its deformed shape and, thus, the forces arising in structural elements. In particular, the stress state arising in each floor cell is mainly composed of the axial stresses in both the main directions of the floor, while the in-plane shear stresses are negligible. As a consequence, the simplified method described in Section 2.1 can be adopted to determine the in-plane transverse stiffness of the equivalent shell elements in their main directions in order to effectively reproduce the actual in plane-stiffness of floor cells.

2.2.2. Determination of Shell Element Properties through the Simplified Method

The thickness h_s of the shell elements used to reproduce the in-plane deformability of floors is set equal to 8 cm, such as that of the roof upper slab. The in-plane stiffness of the shell elements in the joists' direction, derived from Equation (3) by adding the contribution of the predalles slab area A_p, is

$$k_{eq,j} = E_c \cdot (A_s + A_j + A_p) \tag{6}$$

Considering a floor strip of unit width, by applying (5), we obtain the stiffness modifier

$$k_{mod} = (h_s + h_j \cdot n + h_p)/h_s \tag{7}$$

where h_j and h_p are the joists and predalles slab thickness, respectively, while n is the number of joists in the unit strip. For the case study, we find k_{mod} = 1.8.

Conversely, in the direction orthogonal to the joists, the only contribution to the in-plane floor stiffness is provided by the top RC slab. Actually, predalles slabs are not able to contribute to the transmission of axial stresses because of the physical discontinuity between two adjacent slabs. Hence, the in-plane stiffness of the equivalent 2D elements coincides with that of the real floor.

2.2.3. Results

The effect of floor in-plane stiffness with shell elements, determined as described in Section 2.2.2, was investigated under the gravitational loads. In the FE model, the cracking effect on beams flexural stiffness is accounted for by using properly reduced second moments of the area. Moreover, the long-term effects of concrete creep are taken into account through a reduced value of E_c.

From the results of the analyses of the two FE models with and without the equivalent 2D elements, it could be observed that the most relevant effect is on the stresses acting in the circular-shaped RC beam. In presence of shell elements, stresses are about 15% lower than those obtained from the FE model that does not take into account the floor in-plane stiffness.

With regard to the internal forces (normal compression and bending moment) in the top beams of the radial trusses, it can be deduced that accounting for floor in-plane stiffness

induces a slight reduction of stresses of about 7% both in the concrete and in HEA200 steel profiles.

3. Theoretical Basis

The nodes at the beams' intersection in the FE model of the one-way joists floor are referred to, in the following, as vertex nodes, and are marked with a circle in Figure 5.

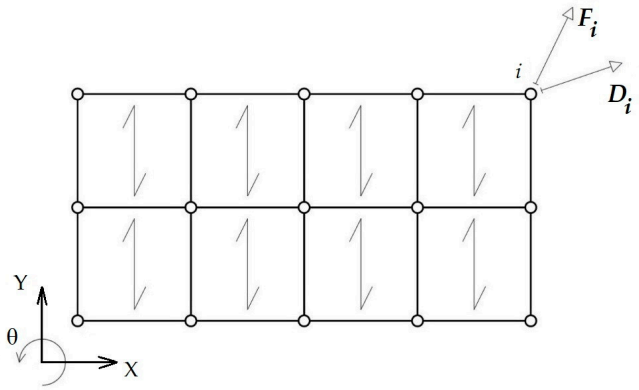

Figure 5. Schematic representation of a floor in the building FE model.

In the structural analysis, the floor behavior is fully described by the relationship between forces applied at vertex nodes and their displacements. For this reason, to adequately define the membrane elements' properties, the equivalence between the solid FE model (3D model) and the 2D FE model (2D model) of the floor must be imposed in terms of the vertex nodes' force–displacement relation.

With restricted attention to the in-plane behavior, the kinematics of each vertex node of is fully described by two translations D_{iX} and D_{iY}, which are parallel to the X and Y directions, respectively, and the rotation $D_{i\theta}$ around the axis orthogonal to the floor middle plane—as shown in see Figure 5—and collected in the 3-vector

$$\boldsymbol{D_i} = [D_{iX},\ D_{iY},\ D_{i\theta}]^{\mathrm{T}} \tag{8}$$

Analogously, the in-plane actions at each vertex node are described by two mutually orthogonal forces F_i and F_{iY} and by torque $F_{i\theta}$, collected in the 3-vector

$$\boldsymbol{F_i} = [F_{iX},\ F_{iY},\ F_{i\theta}]^{\mathrm{T}} \tag{9}$$

Generalized displacements of all vertex nodes are collected in a generalized displacement vector $\boldsymbol{D}$

$$\boldsymbol{D}= \begin{bmatrix} \boldsymbol{D_1} \\ \boldsymbol{D_2} \\ \vdots \\ \boldsymbol{D_N} \end{bmatrix} \tag{10}$$

and, analogously, generalized forces are collected in the generalized force vector $\boldsymbol{F}$

$$\boldsymbol{F}= \begin{bmatrix} \boldsymbol{F_1} \\ \boldsymbol{F_2} \\ \vdots \\ \boldsymbol{F_N} \end{bmatrix} \tag{11}$$

The relationship between generalized displacements and forces is given by

$$\boldsymbol{F} = \boldsymbol{KD} \tag{12}$$

where $\boldsymbol{K}$ is the symmetrical 3 N × 3 N floor in-plane stiffness matrix.

Equation (12) also applies to floor FE models in which floor cells and boundary beams are discretized in finite elements with smaller dimensions (Figure 6) in order to enforce the displacement compatibility.

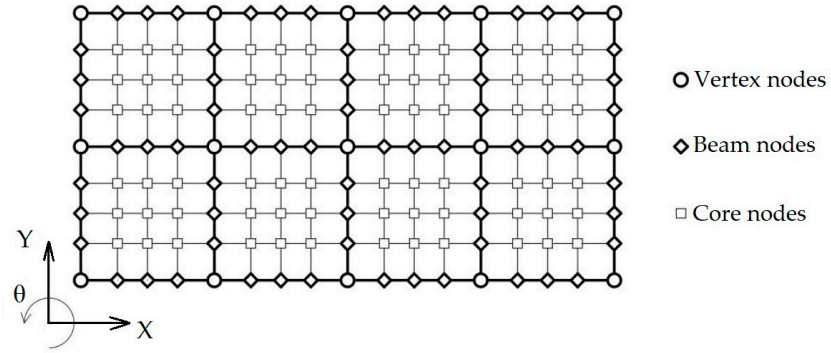

Figure 6. Discretization of floor cells and contouring beams through FE with smaller dimensions.

The cell internal nodes are called core nodes while the internal beam nodes are called beams nodes.

With label *V* for vertex nodes, *B* for beam nodes, and *C* for core nodes, Equation (12) transforms into

$$\begin{bmatrix} \boldsymbol{F_V} \\ \boldsymbol{F_B} \\ \boldsymbol{F_C} \end{bmatrix} = \begin{bmatrix} \boldsymbol{K_{VV}} & \boldsymbol{K_{VB}} & \boldsymbol{K_{VC}} \\ & \boldsymbol{K_{BB}} & \boldsymbol{K_{BC}} \\ Sym. & & \boldsymbol{K_{CC}} \end{bmatrix} \begin{bmatrix} \boldsymbol{D_V} \\ \boldsymbol{D_B} \\ \boldsymbol{D_C} \end{bmatrix} \tag{13}$$

where $\boldsymbol{F_V}$, $\boldsymbol{F_B}$, and $\boldsymbol{F_C}$ are the generalized forces acting at vertex, beam, and core nodes, respectively; $\boldsymbol{D_V}, \boldsymbol{D_B}$, and $\boldsymbol{D_C}$ are the generalized displacements of vertex, beam, and core nodes, respectively; and $\boldsymbol{K_{VV}}, \boldsymbol{K_{BB}}, \boldsymbol{K_{CC}}, \boldsymbol{K_{VB}}, \boldsymbol{K_{VC}}$, and $\boldsymbol{K_{BC}}$ are the suitable submatrices of $\boldsymbol{K}$.

Under the additional assumption that the masses are lumped at vertex nodes, the inertial forces acting on the floor cells are applied only at the vertex nodes. Hence, generalized forces at beam and core nodes vanish and (13) become

$$\begin{cases} \boldsymbol{F_V} = \boldsymbol{K_{VV}}\boldsymbol{D_V} + \boldsymbol{K_{VB}}\boldsymbol{D_B} + \boldsymbol{K_{VC}}\boldsymbol{D_C} \\ \boldsymbol{0} = \boldsymbol{K_{BV}}\boldsymbol{D_V} + \boldsymbol{K_{BB}}\boldsymbol{D_B} + \boldsymbol{K_{BC}}\boldsymbol{D_C} \\ \boldsymbol{0} = \boldsymbol{K_{CV}}\boldsymbol{D_V} + \boldsymbol{K_{CB}}\boldsymbol{D_B} + \boldsymbol{K_{CC}}\boldsymbol{D_C} \end{cases} \tag{14}$$

Since the last two equations are homogeneous, the static condensation method is used to express $\boldsymbol{D_B}$ and $\boldsymbol{D_C}$ as functions of $\boldsymbol{D_V}$. In particular, from the third equation of system (14), we obtain

$$\boldsymbol{D_C} = -\boldsymbol{K_{CC}}^{-1}\boldsymbol{K_{CV}}\boldsymbol{D_V} - \boldsymbol{K_{CC}}^{-1}\boldsymbol{K_{CB}}\boldsymbol{D_B} \tag{15}$$

Using (15) in the second equation of system (14), we obtain

$$\left[\boldsymbol{K_{BV}} - \boldsymbol{K_{BC}}\boldsymbol{K_{CC}}^{-1}\boldsymbol{K_{CV}}\right]\boldsymbol{D_V} + \left[\boldsymbol{K_{BB}} - \boldsymbol{K_{BC}}\boldsymbol{K_{CC}}^{-1}\boldsymbol{K_{CB}}\right]\boldsymbol{D_B} = \boldsymbol{0} \tag{16}$$

and thus

$$\boldsymbol{D_B} = -\left[\boldsymbol{K_{BB}} - \boldsymbol{K_{BC}}\boldsymbol{K_{CC}}^{-1}\boldsymbol{K_{CB}}\right]^{-1}\left[\boldsymbol{K_{BV}} - \boldsymbol{K_{BC}}\boldsymbol{K_{CC}}^{-1}\boldsymbol{K_{CV}}\right]\boldsymbol{D_V} \tag{17}$$

Similarly, we obtain

$$\boldsymbol{D_C} = -\left[\boldsymbol{K_{CC}} - \boldsymbol{K_{CB}}\boldsymbol{K_{BB}}^{-1}\boldsymbol{K_{BC}}\right]^{-1}\left[\boldsymbol{K_{CV}} - \boldsymbol{K_{CB}}\boldsymbol{K_{BB}}^{-1}\boldsymbol{K_{BV}}\right]\boldsymbol{D_V} \tag{18}$$

Substituting (17) and (18) in the first equation of system (14), we obtain an expression of $\boldsymbol{F_V}$ involving only $\boldsymbol{D_V}$ as

$$\boldsymbol{F_V} = \boldsymbol{K} * \boldsymbol{D_V} \tag{19}$$

Then, the same method can be applied to the analysis of a single floor cell (Figure 7), where the number of vertex nodes reduces to 4 (Figure 8). Recalling that each node has 3 DOFs, both the displacement vector $\boldsymbol{D}$, given by Equation (10), and the force vector $\boldsymbol{F}$, given by Equation (11), have 12 components.

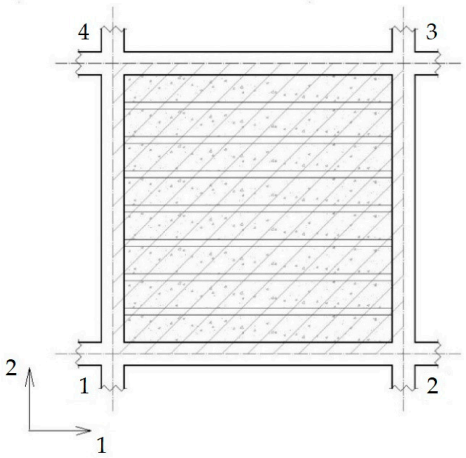

Figure 7. Floor cell.

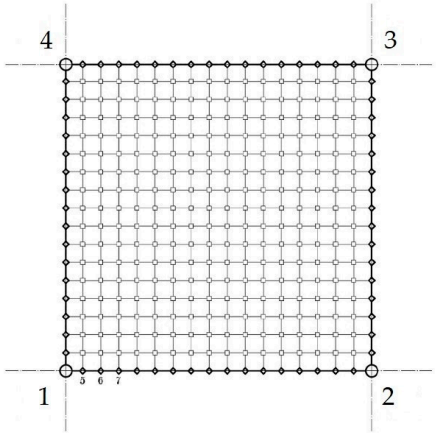

Figure 8. Floor cell FE model.

Hence, the statically reduced stiffness matrix $\boldsymbol{K}$ of the floor cell is a symmetrical 12 × 12 matrix. The floor cell in-plane behavior can then be described by the following system of equations:

$$\begin{bmatrix} F_{11} \\ F_{12} \\ \vdots \\ F_{43} \end{bmatrix} = \begin{bmatrix} K_{11} & K_{12} & \cdots & K_{112} \\ K_{21} & K_{22} & \cdots & K_{212} \\ \vdots & \vdots & \ddots & \vdots \\ K_{41} & K_{42} & \cdots & K_{11} \end{bmatrix} \begin{bmatrix} D_{11} \\ D_{12} \\ \vdots \\ D_{43} \end{bmatrix} \tag{20}$$

It is easy to recognize that the floor cell stiffness is given by two contributions: the one of the beams and the one of the internal floor elements (i.e., RC slab, RC joists, and lightening elements). Hence, the stiffness matrix can be decomposed as the sum of two stiffness matrices

$$\boldsymbol{F} = \boldsymbol{KD} = \left[\boldsymbol{K}^{(B)} + \boldsymbol{K}^{(I)}\right]\boldsymbol{D} \tag{21}$$

where $\boldsymbol{K}^{(B)}$ accounts for the beams' contribution while $\boldsymbol{K}^{(I)}$ accounts for the internal elements' contribution.

From a more detailed perspective, the composition of these two matrices can be expressed as

$$\boldsymbol{K}^{(B)} = \begin{bmatrix} \boldsymbol{K_{VV}}^{(B)} & \boldsymbol{K_{VB}}^{(B)} & \mathbf{0} \\ & \boldsymbol{K_{BB}}^{(B)} & \mathbf{0} \\ Sym. & & \mathbf{0} \end{bmatrix} \tag{22}$$

and

$$\boldsymbol{K}^{(I)} = \begin{bmatrix} \boldsymbol{K_{VV}}^{(I)} & \boldsymbol{K_{VB}}^{(I)} & \boldsymbol{K_{VC}}^{(I)} \\ & \boldsymbol{K_{BB}}^{(I)} & \boldsymbol{K_{BC}}^{(I)} \\ Sym. & & \boldsymbol{K_{CC}}^{(I)} \end{bmatrix} \tag{23}$$

and, by static condensation

$$\boldsymbol{F_V} = \left[\boldsymbol{K_{VV}}^{(B)} + \boldsymbol{K_{VV}}^{(I)} - \boldsymbol{K_{VV}}^{(BI)}\right]\boldsymbol{D_V}. \tag{24}$$

Then, if only the stiffness contribution of the beams on the floor cell perimeter is considered, (24) reduces to

$$\boldsymbol{F_V}^{(B)} = \left[\boldsymbol{K_{VV}}^{(B)} - \boldsymbol{K_{VB}}^{(B)}{\boldsymbol{K_{BB}}^{(B)}}^{-1}\boldsymbol{K_{BV}}^{(B)}\right]\boldsymbol{D_V} \tag{25}$$

Now, it is possible to ideally quantify the stiffness contribution given by only the internal floor elements, $\boldsymbol{\Delta F_V}^{(BI)}$ as

$$\boldsymbol{\Delta F_V}^{(BI)} = \boldsymbol{F_V} - \boldsymbol{F_V}^{(B)} = \boldsymbol{\Delta K}^{(BI)}\boldsymbol{D_V} \tag{26}$$

where

$$\boldsymbol{\Delta K}^{(BI)} = \boldsymbol{K_{VV}}^{(I)} + \boldsymbol{K_{VB}}^{(B)}{\boldsymbol{K_{BB}}^{(B)}}^{-1}\boldsymbol{K_{BV}}^{(B)} - \boldsymbol{K_{VV}}^{(BI)} \tag{27}$$

From (24), it can be observed that the stiffness contribution of the beams and internal floor elements are not uncoupled, and thus the solution cannot be expressed by the sum of the internal floor contribution and the beams' contribution.

The method described above can be applied also to the equivalent 2D membrane model. Actually, it is also possible in this case to identify the stiffness contribution given by beams, $\boldsymbol{K}^{(B)}$, and that of the membrane, $\boldsymbol{K}^{(M)}$. Thus, the system of equations can be written as follows:

$$\boldsymbol{F} = \boldsymbol{KD} = \left[\boldsymbol{K}^{(B)} + \boldsymbol{K}^{(M)}\right]\boldsymbol{D} \tag{28}$$

Similarly to what was derived for the floor cell FE model with solid elements and expressed by Equation (26), the solely internal element stiffness contribution given by the membrane is

$$\boldsymbol{\Delta F}^{(BM)} = \boldsymbol{\Delta K}^{(BM)}\boldsymbol{D_V} \tag{29}$$

The difference between the equivalent 2D membrane model and the 3D solid-element model is that in the 2D model, the internal floor elements (i.e., RC slab, RC joists, and lightening elements) are modeled through the membrane, which is made with homogeneous orthotropic material, while in the 3D model, they are modeled using elements with different material and geometrical properties.

In order for the membrane elements to reproduce the in-plane behavior of the internal floor modeled with solid elements, the elastic properties and thickness h of the membrane elements should be determined by imposing the equality between the stiffness matrices related to the internal floor elements of the 2D and 3D model as follows:

$$\boldsymbol{\Delta K}^{(BM)} = \boldsymbol{\Delta K}^{(BI)} \tag{30}$$

This condition is difficult to achieve unless the real floor is an orthotropic slab itself. Actually, the real floor stiffness is described by a symmetric 12 × 12 matrix, $\mathbf{\Delta K}^{(BI)}$, characterized by 78 components, while the equivalent homogeneous orthotropic membrane is described by only 4 independent terms depending on 5 parameters. These terms are $h{\cdot}E_1$, $h{\cdot}E_2$, $h{\cdot}G_{12}$, and ν_{12}, where E_1 and E_2 are the Young's moduli parallel and orthogonal to the RC joists' direction, respectively (Figure 7), G_{12} is the in-plane shear modulus, and ν_{12} is the Poisson ratio.

Since equality (27) cannot be exactly satisfied, the best thing we can do is to minimize the difference $\mathbf{\Delta F}^{(BI)} - \mathbf{\Delta F}^{(BM)}$ between the forces at vertex nodes for some suitable displacement modes of the floor cell; that is, to minimize the quantity

$$\varepsilon = \left\| \mathbf{\Delta F}^{(BI)} - \mathbf{\Delta F}^{(BM)} \right\|^2 = \left[\mathbf{\Delta K}^{(BI)} - \mathbf{\Delta K}^{(BM)} \right] \boldsymbol{D_V}{\cdot}\boldsymbol{D_V} = \boldsymbol{E}\boldsymbol{D_V}{\cdot}\boldsymbol{D_V} \tag{31}$$

with respect to the free parameters $h{\cdot}E_1$, $h{\cdot}E_2$, $h{\cdot}G_{12}$, and ν_{12}. With the influence of ν_{12} on the in-plane behavior of the floor being initially neglected, the deformation patterns chosen to evaluate the equivalent membrane properties are those shown in Figure 9.

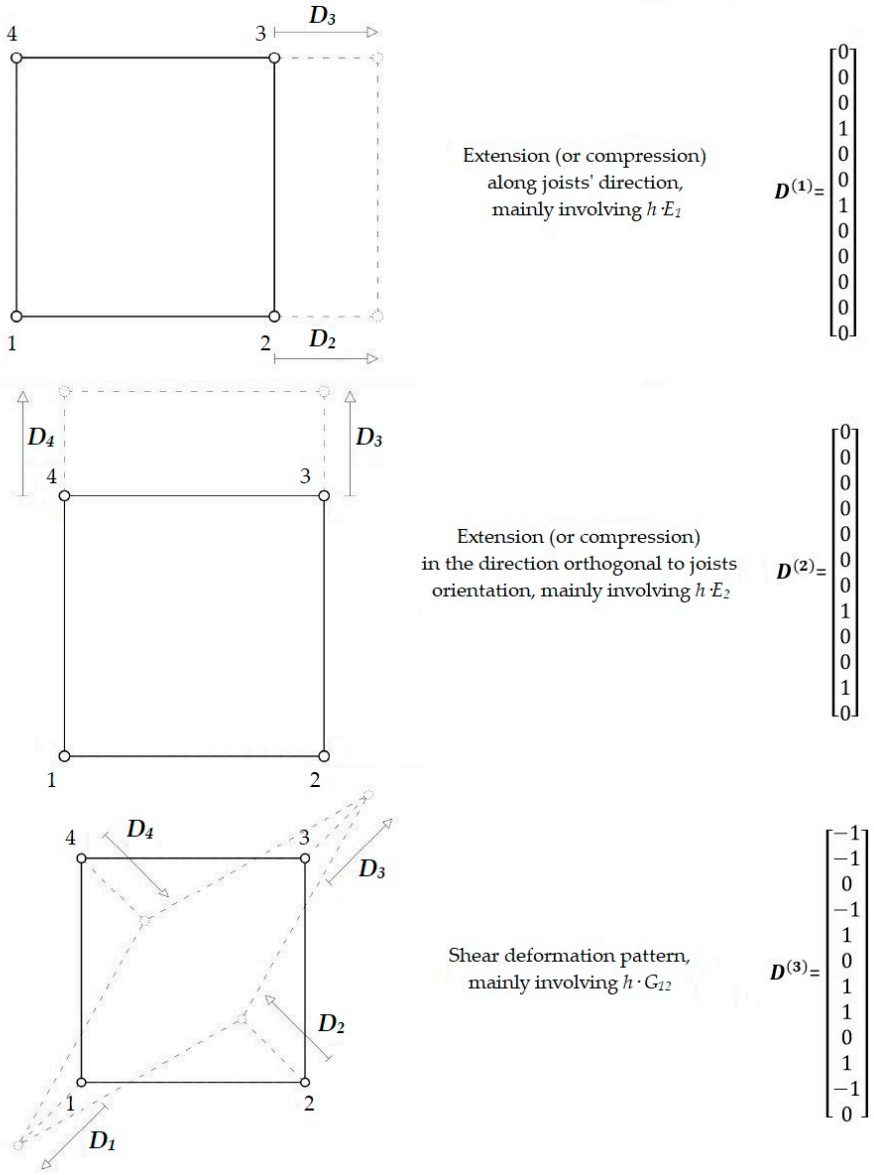

Figure 9. Deformation patterns.

The first deformation pattern is a pure extension along the joists' direction, the second one is a pure extension in the orthogonal direction, and the third one is a pure shear deformation. Then, ε can be quantified by the following sum

$$\widetilde{\varepsilon} = \boldsymbol{E}\,\boldsymbol{D}^{(1)}\cdot\boldsymbol{D}^{(1)} + \boldsymbol{E}\,\boldsymbol{D}^{(2)}\cdot\boldsymbol{D}^{(2)} + \boldsymbol{E}\,\boldsymbol{D}^{(3)}\cdot\boldsymbol{D}^{(3)} \tag{32}$$

where $\boldsymbol{D}^{(1)}$, $\boldsymbol{D}^{(2)}$, and $\boldsymbol{D}^{(3)}$ are the vectors of the generalized displacements of vertex nodes for the three deformation patterns shown in Figure 9.

In practice, to minimize $\widetilde{\varepsilon}$, the method based on the search of the equality between the vertex nodes' displacements obtained by the 2D and 3D models is adopted. In particular, when the vertex nodes' displacements under a deformation pattern are similar, within a tolerance, for the two models, the value of the equivalent membrane parameter associated with the considered deformation pattern accurately describes the behavior of the real floor under that pattern.

The method described above is based on the classic homogenization approach of a microscopically inhomogeneous material.

4. FE-Based Method

The method is derived from the theory described in Section 3. It allows for the determination of the elastic properties of the homogeneous material constituting the 2D elements used to reproduce the in-plane stiffness of single floor cells. In particular, the equivalence condition is ideally achieved when, for each deformation pattern, the most significant displacements of the vertex nodes are equal, within a tolerance, in the two models.

In the following section, the static schemes used to obtain the deformation patterns mentioned in Section 3 are described.

4.1. Static Schemes

Hereafter, three static schemes are considered. Each static scheme is chosen to analyze the following deformation patterns (also called deformation modes):

- MODE 1: shear deformation mode;
- MODE 2: extension along *X* axis, parallel to joists' direction;
- MODE 3: extension along *Y* axis, orthogonal to joists' direction.

To reproduce the shear deformation pattern (MODE 1), the load and restraint configurations shown in Figure 10a are adopted. Note that a pin support is applied to vertex node A, and a roller support preventing translations along X direction is applied to vertex node D. Displacements of the floor cell middle plane orthogonal to the plane are restrained.

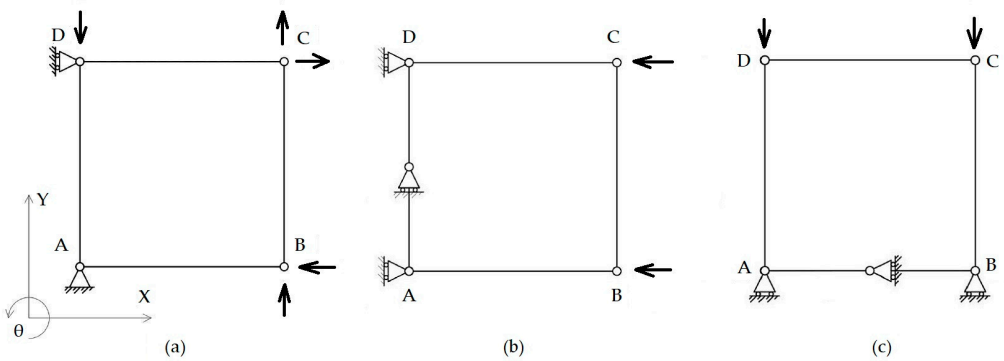

Figure 10. Static schemes of (**a**) MODE 1, (**b**) MODE 2 (**c**) and MODE 3.

Upward forces along Y are applied to vertex nodes B and C, while a downward force is applied to node D. Along X, a rightward force is applied to node C while a leftward force is applied to node B.

In MODE 2 (Figure 10b), two roller supports preventing translations along X are applied to nodes B and C, and a roller support preventing translation along Y is applied at the midpoint of the floor edge AD. This roller guarantees that the deformed shape of the floor cell is symmetric with respect to the axis passing through the midpoints of edges AD and BC.

Finally, MODE 3 (Figure 10c) is obtained by applying roller supports to nodes A and B to prevent displacements along Y direction. Similarly to MODE 2, a roller support is also applied to the midpoint of floor edge AB in order to prevent translations of this point along X direction and guarantee the symmetry with respect to the axis passing through the midpoints of edges AB and DC.

4.2. Application of Loads and Restraints to the 3D Model

In the 2D model of the floor, the perimeter beams are represented through one-dimensional frame elements, and the intersection between two perimeter beams is identified by a single point, called the vertex node.

Conversely, in the solid elements model (3D model), the floor cell is represented with its 3D geometry and, consequently, the intersection between two adjacent beams is a parallelepiped solid region whose edges are highlighted by the green color in Figure 11. At intersection regions, loads are applied to the two vertical cross-sections of the parallelepiped aligned with the longitudinal axes of the two converging beams; see the red hatched planes in Figure 11.

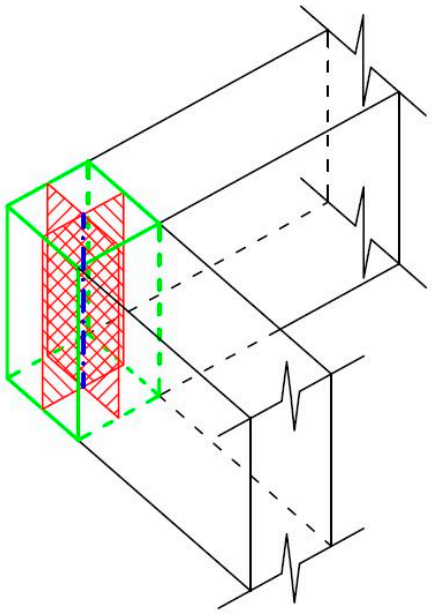

Figure 11. Parallelepiped constituting the intersection between two adjacent beams in the floor cell model made by solid finite elements.

With it being taken into account that, in the model, perimeter beams are discretized in smaller finite solid elements through a mesh, it follows that loads at intersection regions are applied to the mesh nodes belonging to the parallelepiped vertical cross-sections mentioned above, as shown in Figure 12 for one of the two parallelepiped cross-sections.

On the basis of what has been discussed, it can be gathered that the loads acting at vertex nodes along X or Y direction are applied to the mesh nodes belonging to the parallelepiped vertical cross-section orthogonal to the load direction.

Roller supports, preventing translations along one of the two principal horizontal directions of the floor cell and vertical displacements, are also applied to the mesh nodes belonging to the parallelepiped vertical cross-section parallel to the horizontal direction in which translations are allowed. Regarding the pin supports present in the static scheme

of MODE 1 (Figure 10), they are applied to the mesh nodes belonging to the vertical segment of the parallelogram constituting the intersection between the vertical cross-sections mentioned above. This segment is highlighted in blue in Figure 11.

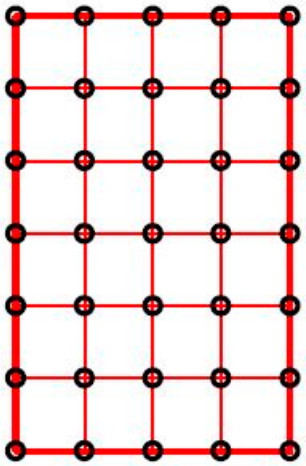

Figure 12. Mesh nodes in a vertical cross-section of the parallelepiped, to which loads and restraints are applied at intersection regions.

Finally, the displacement along X or Y direction at intersection regions is obtained from the average of the displacement values along X or Y, respectively, of the mesh nodes belonging to the vertical cross-sections of the parallelepiped constituting the considered intersection region.

4.3. Operating Procedure

The proposed procedure is articulated in the following steps:

1. Realization of the floor cell model, including the perimeter beams, using solid finite elements. Each element constituting the floor cell is modeled with its actual dimensions and with the elastic properties of the material of which it is made. This model is built to reproduce the actual behavior of the floor cell.
2. Realization of the floor cell model, including the perimeter beams, using frame elements for the beams and 2D elements with the membrane behavior for the floor. The geometry is congruent with that of the 3D model. In particular, the side length of the 2D element is equal to the distance, in the 3D model, between the longitudinal axes of the perimeter beams orthogonal to that side. This condition guarantees that the distances between the longitudinal axes of the perimeter beams in the 2D model are equal to those in the 3D model. Perimeter beams are modeled with their actual cross-section and with the elastic properties of the concrete of which they are constituted, used also in the 3D model. The thickness of the 2D elements has to be chosen, and a homogenized material with orthotropic elastic behavior has to be defined, with initial values of the unknown equivalent elastic properties being set. Herein, for RC floors with joists, the thickness is set equal to that of the RC slab, while the initial values of the homogenized material elastic properties are set equal to those of the concrete constituting the real slab.
3. Application to loads and restraints of the static scheme of MODE 1 to both the 2D and 3D model. The applied forces are equal to 707 kN so that the resultant load applied to each vertex node is equal to 1000 kN. Then, the values of the displacement components parallel to Y at vertex nodes B and C obtained from the two models are compared. If the differences between these displacement components are greater than a fixed tolerance, which is herein taken to be equal to 1%, it is necessary to modify the elastic shear modulus G_{xy} of the 2D elements by raising or decreasing its value. Then, the analysis of the 2D model is carried out again and similarly to what was

done previously, the comparison of displacement components is performed. Thus, the value of G_{xy} is determined through an iterative procedure ended once the differences between the displacement components mentioned above are smaller than the fixed tolerance. The 2D model is then updated, with the value of G_{xy} obtained at the end of the iterative procedure.

4. Similarly to what done in step 3 for MODE 1, the 2D and 3D models of the floor cell are now analyzed under the static scheme of MODE 2. In this case, the load magnitude applied to nodes B and C is taken equal to 500 kN in order to apply, in X direction, a total force equal to 1000 kN. The values of the displacement components parallel to X at vertex nodes B and C obtained from the two models are compared. If the percentage difference between these displacement components is greater than a fixed tolerance, which is herein taken to be equal to 1%, it is necessary to modify the elastic modulus along X of the homogeneous material, E_x, by raising or decreasing its value. At the end of this second iterative procedure, the 2D element is characterized by the equivalent values of G_{xy} and E_x.
5. Finally, in consideration of the static scheme of MODE 3 and to search for the equality of the displacement components parallel to Y at vertex nodes C and D obtained from the two FE models, the equivalent value of E_y is determined. Moreover, from the comparison of displacement components parallel to X at vertex nodes B and C obtained from the two FE models, the value of ν_{yx} is determined. Similarly to what was done for MODE 2, the load magnitude applied to nodes C and D can be taken to be equal to 500 kN. The considered deformation modes (MODE 1, MODE 2 and MODE 3) are not independent among them since the elastic parameter of the orthotropic material mainly involved in one mode influences the 2D element behavior also under the other deformation modes. Hence, further analyses are required to check if the differences between the displacement components, obtained from the two models in steps 3, 4, and 5, are still smaller than the fixed tolerance. If one of these steps is not satisfied, the parameter determined in that step has to be modified until convergence is achieved.

4.4. Application of the Method to a Case Study

A floor cell of typology and geometric characteristics typical of the Italian RC school buildings constructed between the 1950s and the 1970s was chosen. To identify these characteristics, a set of 18 existing schools located in the middle and south of Italy was investigated. From this survey, it was found that the most used floor typology is that constituted by RC joists and an RC slab on the top as structural elements, with ceiling bricks and lightening elements (Figure 13).

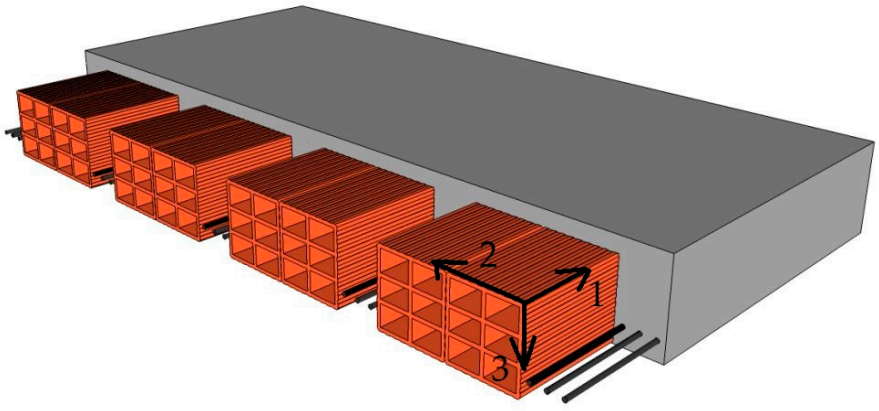

Figure 13. Most used floor typology in the set of existing Italian RC schools considered in the survey.

The geometric characteristics of the elements constituting the floor cell considered were following:

- Floor with a 408 × 408 cm^2 plane size;
- Perimeter beams with a 30 × 52 cm^2 cross-section;
- A 4 cm thick RC slab;
- RC joists with a 12 × 20 cm^2 cross-section;
- Ceiling bricks 48 × 15 × 20 cm^3 in size.

4.4.1. Material Properties

For the perimeter beams, the slab, and the joists, the mechanical properties of concrete strength class C25/30 are adopted. Thus, the Young's modulus E = 31,476 MPa, the Poisson ratio ν = 0.2, and the shear elastic modulus G = 13,115 MPa are adopted.

The ceiling bricks, in the model with solid finite elements, are modeled with solid elements (i.e., without holes) made of a homogenized orthotropic material, equivalent to real ceiling bricks. In particular, the elastic properties of hollow bricks produced with outdated technologies are adopted. These properties are derived from the experimental test results reported in [38].

Some considerations have to be made on the choice of G_{12}. The transmission of shear stresses between the bricks and the RC elements of the floor, i.e., the slabs and the joists, relies on the grip due to the scratches on the bricks' surfaces. Since, under horizontal actions, ceiling bricks are not fully adhered to the joists and the slab, it is cautiously assumed that the transmission of shear stress between the bricks and the surrounding concrete is negligible; hence, G_{12} = 0.1 MPa.

The elastic properties of the homogenized orthotropic material of ceiling bricks used in the 3D model are reported in Table 1, where E_1 is the Young's modulus parallel to bricks' holes, and E_2 is the Young's modulus orthogonal to the holes.

Table 1. Elastic properties of the homogenized orthotropic material constituting the equivalent solid bricks used in the 3D model to reproduce the real hollow ceiling bricks.

E_1 (MPa)	E_2 (MPa)	E_3 (MPa)	G_{12} (MPa)	G_{23} (MPa)	ν_{12}	ν_{21}
6970	4000	4000	0.1	0.1	0.2	0.115

4.4.2. FE Models

The two FE models of the floor cell considered as a case study were made using SAP2000 software [39]. The 3D model was realized according to step 1 of the method described in Section 4.3. In particular, for both ceiling bricks and RC elements of the floor, solid FE with dimensions 6 × 6 × 4 cm^3 were used, while for the perimeter beams, solid FE with dimensions 6 × 5 × 4 cm^3 or 5 × 6 × 4 cm^3 were used, respectively, for beams parallel to the X or Y direction. In the intersection regions, solid elements 5 × 5 × 4 cm^3 in size were used. The beams were modeled with the extrados coplanar to that of the slab. Out-of-plane displacements of the floor cell were restrained at the slab top surface.

The 2D model was realized according to step 2 of the method described in Section 4.3. In particular, the thickness of membrane elements is set equal to that of the floor RC slab, i.e., 4 cm. For the elastic properties of the homogenized material constituting 2D elements, those reported in Section 4.4.1 for concrete C25/30 are adopted.

The mesh size was chosen according to a sensitivity analysis in which the mesh size was reduced until the floor displacement of the 2D model under in-plane compression loads had a maximum scatter of 1% with respect to a fitter mesh. A discretization with 16 × 16 square finite elements was adopted.

4.4.3. Discussion of Results

The elastic properties of the homogenized material constituting the equivalent 2D elements of the case study obtained with the operating procedure described in Section 4.3 are reported in Table 2.

From the comparison of these properties with those of C25/30 concrete (cf. Section 4.4.1) adopted for the RC elements of the considered case study, it can be concluded that the contribution of joists and ceiling bricks to the axial in-plane stiffness of the floor cell is greater in the direction of the joists (X), as expected.

Table 2. Elastic properties of the homogenized orthotropic material of the equivalent 2D elements obtained for the considered case study.

E_x (MPa)	E_y (MPa)	G_{xy} (MPa)	ν_{xy}	ν_{yx}
45,200	35,300	14,500	0.2	0.26

In this direction, the Young's modulus of the homogenized material, E_x, is equal to 42,000 MPa, roughly 33% higher than that of concrete (31,476 Mpa). Since in the 2D model, the thickness of membrane elements is equal to that of the floor's slab, it follows that the 33% increase is due to the axial in-plane stiffness of joists and ceiling bricks.

In the analysis performed, the contribution of ceiling bricks to the in-plane shear stiffness of floor elements was neglected, reasonably assuming that, in real conditions, ceiling bricks are probably not fully adhered to the RC joists and the slab. Hence, only the contributions of the slab and joists were considered. Comparing the shear modulus of the homogenized orthotropic material (Table 2) with that of concrete C25/30, we can observe that the former is about 10% higher than the latter. Since, as stated above, in the 2D model, the thickness of membrane elements is equal to that of the floor's slab, it follows that the 10% increase is due to the joists' shear stiffness. Therefore, it can be gathered that the main contributor to the floor in-plane shear stiffness the RC slab. Since under seismic actions, floors are subject mainly to shear strains, it can be concluded that the simplified analytical-based method described in Section 2.1 is adequate to reproduce the in-plane stiffness of RC floors with lightening elements when the thickness of shell elements is set equal to that of the RC slab of the floor.

To compare the numerical procedure with the simplified analytical-based method proposed in Section 2.1, it was applied to the case study described in Section 2.2. The elastic properties of the equivalent shell elements with a thickness equal to 8 cm are reported in Table 3.

Table 3. Elastic properties of the homogenized orthotropic material of the equivalent 2D elements obtained for the case study described in Section 2.2.

E_x (MPa)	E_y (MPa)	G_{xy} (MPa)	ν_{xy}	ν_{yx}
51,935	31,950	33,500	0.2	0.26

Comparing the stresses in structural elements obtained from the FE model built with shell elements with the properties described in Table 3 to those obtained from the model described in Section 2.2, we can observe that the differences are practically negligible. In particular, the reduction of stresses in the circular-shaped RC beam was 14.8%, while with the simplified method, a 15% reduction was obtained. With regard to the stresses in the top beams of the radial trusses, both in the concrete and in HEA200 steel profiles, a reduction of 6.7% instead of 7% was obtained. Therefore, the results obtained for the considered case study from the numerical procedure are fundamentally equal to those obtained from the simplified analytical-based method.

5. Conclusions

In this paper, the simplified analytical-based method sometimes adopted by engineers to reproduce in-plane deformability of orthotropic floors, based on the equality of in-plane

stiffness of the real floor and the equivalent shell elements, is provided. In particular, it has been outlined that the equivalence is imposed only on the normal in-plane stiffness, with the in-plane shear behavior being neglected. As a consequence, the equivalent shell elements obtained from the simplified method may not be suitable to reproduce the actual in-plane stiffness of floors under seismic actions.

Nonetheless, it was observed that it may be useful to reproduce the in-plane stiffness of floors in inclined roofs under static loads. A real case study in which the simplified method was used to reproduce in-plane deformability of floors under gravitational loads is presented. From the analysis of the case study in the presence and absence of the equivalent shell elements, it was observed that the floor's in-plane stiffness has a non-negligible effect on the structural elements' stress state.

Subsequently, an advanced FE-based method to reproduce the actual in-plane stiffness of floors in the FE model of the building through equivalent shell elements with prevalent membrane behavior has been proposed.

This method is particularly useful for complex RC floor systems, such as one-way joists systems with lightening elements.

The method, inspired by homogenization procedures, exploits the fact that in the FE model of the floor, the interaction between frame and shell elements takes place in the corresponding beams' intersection nodes.

The method consists in modelling the floor cell using both a 3D solid FE model and a 2D model with frame and shell elements with a prevalent membrane behavior. The elastic properties of the shell homogenized orthotropic material are determined with the aim of finding the equality of the cell vertex node displacements in the two models for three significant deformation patterns of the floor cell.

Author Contributions: Conceptualization, G.F. and M.P.; methodology, I.P. and G.F.; software, G.F. and S.B.; validation, G.F. and M.P.; formal analysis, I.P.; investigation, G.F.; resources, M.P.; data curation, G.F.; writing—original draft preparation, G.F.; writing—review and editing, G.F.; visualization, G.F.; supervision, M.P. and I.P.; project administration, M.P.; funding acquisition, M.P. All authors have read and agreed to the published version of the manuscript.

Funding: The research was partially funded by the Italian Department of Civil Protection within the framework of Executive Project DPCReLUIS 2022–2024 and the European Union Next-GenerationEU (PIANO NAZIONALE DI RIPRESA E RESILIENZA (PNRR)—MISSIONE 4 COMPONENTE 2, INVESTIMENTO 1.5—D.D. 1058 23/06/2022, ECS00000043) within the Interconnected Nord-Est Innovation Ecosystem (iNEST). This manuscript reflects only the authors' views and opinions, and neither the European Union nor the European Commission can be considered responsible for them. The strategic plan is supported by the University of Udine within the framework of the "ESPeRT" project, whose support is greatly appreciated.

Institutional Review Board Statement: Not applicable.

Data Availability Statement: No new data were created or analyzed in this study. Data sharing is not applicable to this article.

Conflicts of Interest: The authors declare no conflict of interest.

References

1. Goldberg, J.E.; Herness, E.D. Vibration of multistory buildings considering floor and wall deformations. *BSSA* **1965**, *55*, 181–200. [CrossRef]
2. Saffarini, H.; Qudaimat, M. In-plane floor deformations in RC Structures. *J. Struct. Eng. (NYNY)* **1992**, *118*, 3089–3102. [CrossRef]
3. Ju, S.H.; Lin, M.C. Comparison of building analyses assuming rigid or flexible floors. *J. Struct. Eng. (NYNY)* **1999**, *125*, 25–39. [CrossRef]
4. Pecce, M.R.; Ceroni, F.; Maddaloni, G. In-plane deformability of RC floors: Assessment of the main parameters and influence on dynamic behaviour. *Bull. Earthq. Eng.* **2019**, *17*, 297–311. [CrossRef]
5. Khajehdehi, R.; Panahshahi, N. Effect of openings on in-plane structural behavior of reinforced concrete floor slabs. *J. Build. Eng.* **2016**, *7*, 1–11. [CrossRef]
6. European Committee for Standardization. *Eurocode 8: Design of Structures for Earthquake Resistance—Part 1: General Rules, Seismic Actions and Rules for Buildings*; UNI Ente Nazionale di Unificazione: Milan, Italy, 2005.

7. Ministero delle Infrastrutture e dei Trasporti. *DM 17 Gennaio 2018. Aggiornamento Delle "Norme Tecniche per le Costruzioni"*; Gazzetta Ufficiale: Rome, Italy, 2018; Volume 42. (In Italian)
8. Consiglio Superiore dei Lavori Pubblici. *Circolare 21 Gennaio 2019, n. 7—Istruzioni per L'applicazione Dell'«Aggiornamento delle "Norme Tecniche per le Costruzioni"» di cui al Decreto Ministeriale 17 Gennaio 2018*; Gazzetta Ufficiale: Rome, Italy, 2018. (In Italian)
9. *NZS 1170.5 Supp 1:2004*; Structural Design Actions. Part 5: Earthquake Actions—New Zealand Commentary. Standards New Zealand Standard: Wellington, New Zealand, 2004.
10. Greek Seismic Code. *Earthquake Resistant Design of Structures*; Earthquake Planning and Protection Organization: Athens, Greece, 2000.
11. American Society of Civil Engineers. *Minimum Design Loads for Buildings and Other Structures*, 2nd ed.; ASCE/SEI 7-10; American Society of Civil Engineers: Reston, VA, USA, 2002.
12. *International Building Code (IBC)*; International Code Council: Country Club Hills, IL, USA, 2009.
13. Building Seismic Safety Council of the National Institute of Building Sciences. *NEHRP Recommended Provisions for Seismic Regulations for New Buildings and Other Structures (FEMA 450)—Part 1: Provisions*; Building Seismic Safety Council, National Institute of Building Sciences: Washington, DC, USA, 2003.
14. Miani, M.; Di Marco, C.; Frappa, G.; Pauletta, M. Effects of Dissipative Systems on the Seismic Behavior of Irregular Buildings–Two Case Studies. *Buildings* **2020**, *10*, 202. [CrossRef]
15. Frappa, G.; Pauletta, M. Seismic retrofitting of a reinforced concrete building with strongly different stiffness in the main directions. In Proceedings of the 14th Fib International PhD Symposium in Civil Engineering, Rome, Italy, 5–7 September 2022.
16. Doudoumis, I.N.; Athanatopoulou, A.M. Code provisions and analytical modelling for the in-plane flexibility of floor diaphragms in building structures. *J. Earthq. Eng.* **2001**, *5*, 565–594. [CrossRef]
17. Kunnath, S.; Panahshahi, N.; Reinhorn, A. Seismic response of RC buildings with inelastic floor diaphragms. *J. Struct. Eng. (NYNY)* **1991**, *117*, 1218–1237. [CrossRef]
18. Fleischman, R.B.; Farrow, K.T. Dynamic behavior of perimeter lateral-system structures with flexible diaphragms. *Earthq. Eng. Struct. Dyn.* **2001**, *30*, 745–763. [CrossRef]
19. Tena-Colunga, A.; Abrams, D.P. Seismic behavior of structures with flexible diaphragms. *J. Struct. Eng. (NYNY)* **1996**, *122*, 439–445. [CrossRef]
20. Eivani, H.; Moghadam, A.S.; Aziminejad, A.; Nekooei, M. Effects of diaphragm flexibility on seismic response of asymmetric-plan buildings. *Gradevinar* **2018**, *70*, 965–974. [CrossRef]
21. Moeini, M.; Rafezy, B. Investigation into the Floor Diaphragms Flexibility in Reinforced Concrete Structures and Code Provision. *Glob. J. Res. Eng.* **2011**, *11*, 24–36.
22. Fleischman, R.B.; Farrow, K.T.; Eastman, K. Seismic Performance of Perimeter Lateral-System Structures with Highly Flexible Diaphragms. *Earthq. Spectra* **2001**, *18*, 251–286. [CrossRef]
23. Huber, M.T. Die Grundlagen einer rationellen Bemessung der kreuzweise bewehrten Eisenbetonplatte, Österreichische Ingenieur- und Architekten-Zeitschrift. *Band* **1914**, *66*, 557–564.
24. Troitsky, M.S. *Stiffened Plates: Bending, Stability and Vibrations*; Elsevier: Amsterdam, The Netherlands; Scientific Pub. Co.: New York, NY, USA, 1976.
25. Clyne, T.W.; Hull, D. *An Introduction to Composite Materials*, 3rd ed.; Cambridge University Press: Cambridge, UK, 2019.
26. Biancolini, M.E. Evaluation of equivalent stiffness properties of corrugated board. *Comput. Struct.* **2005**, *69*, 322–328. [CrossRef]
27. Garbowki, T.; Gajewski, T. Determination of Transverse Shear Stiffness of Sandwich Panels with a Corrugated Core by Numerical Homogenization. *Materials* **2021**, *14*, 1976. [CrossRef]
28. Marek, A.; Garbowski, T. Homogenization of sandwich panels. *CAMES* **2015**, *22*, 39–50.
29. Staszak, N.; Garbowski, T.; Ksit, B. Optimal Design of Bubble Deck Concrete Slabs: Sensitivity Analysis and Numerical Homogenization. *Materials* **2023**, *16*, 2320. [CrossRef]
30. Staszak, N.; Garbowski, T.; Szymczak-Graczyk, A. Solid Truss to Shell Numerical Homogenization of Prefabricated Composite Slabs. *Materials* **2021**, *14*, 4120. [CrossRef]
31. Pecce, M.R.; Ceroni, F.; Maddaloni, G.; Iannuzzella, V. Assessment of the in-plane deformability of RC floors with traditional and innovative lightening elements in RC framed and wall structures. *Bull. Earthq. Eng.* **2017**, *15*, 3125–3149. [CrossRef]
32. Ruggieri, S.; Porco, F.; Uva, G. A numerical procedure for modeling the floor deformability in seismic analysis of existing RC buildings. *J. Build. Eng.* **2018**, *19*, 273–284. [CrossRef]
33. Jain, S.K.; Jennings, P.C. Analytical models for low-rise buildings with flexible floor diaphragms. *Earthq. Eng. Struct. Dyn.* **1985**, *13*, 225–241. [CrossRef]
34. Bahar, S.; Benanane, A.; Belarbi, A. The Influence of Deformability of Horizontal Diaphragms in the Distribution of Seismic Loads to Bracing Elements in Rectangular Buildings. *JMES* **2019**, *6*, 105–118.
35. Sadashiva, V.K.; MacRae, G.A.; Deam, B.L.; Spooner, M.S. Quantifying the seismic response of structures with flexible diaphragms. *Earthq. Eng. Struct. Dyn.* **2012**, *41*, 1365–1389. [CrossRef]
36. Aktan, A.E.; Nelson, G.E. Problems in predicting seismic responses of RC buildings. *J. Struct. Eng. (NYNY)* **1988**, *114*, 2036–2056. [CrossRef]
37. *CSI Analysis Reference Manual, SAP2000®, ETABS®, SAFE®, e CSi-Bridge®*; Computers & Structures: Berkeley, CA, USA, 2018.

38. Canal, N. Consorzio Poroton Italia. Resistenza Meccanica di Blocchi Forati a Fori Orizzontali. Available online: https://www.poroton.it/news/1253/resistenza_meccanica_blocchi_forati/ (accessed on 9 September 2021).
39. Wilding, B.V.; Godio, M.; Beyer, K. The ratio of shear to elastic modulus of in-plane loaded masonry. Problems in predicting seismic responses of RC buildings. *Mater. Struct.* **2020**, *53*, 40. [CrossRef]